Journal of Hazardous Materials Advances 20 (2025) 100876

Contents lists available at ScienceDirect

Journal of Hazardous Materials Advances

journal homepage: www.elsevier.com/locate/hazadv

Ternary Fe-Zn-Al layered double-hydroxides for interactive removal of cd and pb from aqueous solutions: Isotherms, kinetics and application to real samples

Ramatsobane Rosy Phogole [a,b], Philani Perfect Mpungose [c], Luthando Nyaba [a,b], Mthokozisi Mnguni [a,b], Philiswa Nosizo Nomngongo [a,b,*]

[a] Department of Chemical Sciences, University of Johannesburg, Doornfontein Campus, P.O. Box 17011, Doornfontein 2028, South Africa
[b] Department of Science, Technology and Innovation-National Research Foundation South African Research Chair Initiative (DSTI-NRF SARChI) in Nanotechnology for Water, University of Johannesburg, Doornfontein 2028, South Africa
[c] Department of Chemistry, Cape Peninsula University of Technology, Cape Town 2000, South Africa

ARTICLE INFO

Keywords:
Fe-Zn-Al LDH
Adsorptive removal
Trace metals, Surface and groundwater

ABSTRACT

The ongoing influx of trace elements in our water systems from industrial wastewater poses a need for water decontamination. In this study, Fe-Zn-Al LDH was synthesised via the co-precipitation method as an adsorbent in the decontamination of Cd and Pb from surface and groundwater. The synthetic technique was used because it is simple and effective. The synthesised Fe-Zn-Al LDH was characterised by instruments including X-ray powder diffraction (P-XRD), transmission electron microscope (TEM), Fourier transform infrared spectroscopy (FTIR) and scanning electron microscope-energy dispersive spectroscopy (SEM-EDS). The FTIR showed that the dominant characteristic groups of Fe-Zn-Al LDH were O—H, CO_3^{2-}, NO_3^-, M-O and M-O-M, which are the expected functional groups. The SEM-EDS confirmed the elemental composition of the material, and XRD also confirmed the lamellar structure of Fe-Zn-Al LDH by having characteristic peaks of LDH. Under optimum conditions, adsorption kinetics and equilibrium studies were conducted to investigate possible adsorption mechanisms involved during the removal process. The kinetics data fitted the Elovich and pseudo-second-order models, with the relatively highest correlation coefficient for both analytes compared to the pseudo-first-order model. It was also observed that the Langmuir and the Freundlich models show the best agreement with adsorption equilibrium data. The maximum adsorption capacities for Cd and Pb were calculated using the Langmuir model equation and were 11.9 and 280 mg/g. Moreover, because of its high adsorption affinity and fast adsorption kinetics, the Fe-Zn-Al LDH proved to be a suitable adsorbent material for Cd and Pb removal from water samples, with removal efficiencies ranging from 80–98 %.

1. Introduction

The influx of hazardous heavy elements into the environmental water systems seriously threatens water quality, aquatic ecosystems and human health. Domestic and industrial wastewater effluents release toxic trace elements, which include arsenic (As), chromium (Cr), cadmium (Cd), cobalt (Co), lead (Pb) and nickel (Ni) (Qasem et al., 2021; Shahabi Nejad and Sheibani, 2022), into environmental water systems such as rivers and dams. These contaminants sometimes exist in levels that exceed the acceptable concentration required by any living organism and thus threaten the aquatic organisms and human health that rely on contaminated water. Some of the effects include the ability of heavy metals to inhibit biological functions and disrupt physiological processes because they have a strong binding affinity toward nitrogen, oxygen, and other biomolecule atoms (Narwal et al., 2023). As a result, the accumulation and excessive intake of heavy metals can cause several diseases, namely, Alzheimer's and Parkinson's diseases, and amyotrophic lateral sclerosis (Momin et al., 2024). Therefore, toxic heavy metals need to be removed from our water systems to protect human health and the environment and maintain the sustainability of the ecosystems (Zlati et al., 2022), which is what this study aimed to achieve.

Some conventional decontamination methods include lime

* Corresponding author.
E-mail address: pnnomngongo@uj.ac.za (P.N. Nomngongo).

https://doi.org/10.1016/j.hazadv.2025.100876
Received 26 May 2025; Received in revised form 22 August 2025; Accepted 1 September 2025
Available online 2 September 2025

coagulation, chemical precipitation, ion exchange, solvent extraction and reverse osmosis (Karim et al., 2023; Yang et al., 2019). However, there are drawbacks to using conventional techniques to remove metal ions from wastewater, such as high reagent and energy requirements, low metal removal, and the creation of hazardous waste that needs to be properly disposed of. Consequently, developing effective and eco-friendly techniques to remediate heavy metals is essential. Adsorption is emerging as the ideal water remediation technique because it is affordable, easy to apply and has high removal performance (Kumar et al., 2023; Madhubashani et al., 2021). The performance and costs of the entire adsorption process majorly depend on the adsorbent material. As a result, it is paramount to employ adsorbents with large sorptive sites that are affordable, easily obtainable, and can be reused several times.

Hydrotalcites (HTs), a class of anionic clays and layered double hydroxides (LDH) with a unique layered structure and remarkable ion-exchange properties, have been used for removing Pb, Cd, Ni, Cr, As, mercury (Hg), copper (Cu), zinc (Zn), and iron (Fe) ions from water (Pastor et al., 2020; Mo et al., 2024; Abushawish et al., 2024; Bordoloi et al., 2013). Its wide application owes to fascinating structure and physicochemical properties such as enhanced surface area and porosity, thermal stability, and tuneable composition. HTs exhibit positively charged brucite-like layers, with the general formula $[M^{2+}_{(1-x)}M^{3+}{}_x(OH)_2]^{x+}[(A^{n-})_{x/n}\bullet yH_2O]^{x-}$, where M^{2+} and M^{3+} are divalent and trivalent metal cations, respectively, and A^{n-} is the interlayer anion (Conterosito et al., 2018). During adsorption, the interlayer anions can be exchanged by the targeted anionic heavy metals, whereas cations are susceptible to cationic exchange by divalent and trivalent heavy metals (Lin et al., 2023; Nguyen et al., 2022). These characteristics make LDHs favoured adsorbents in water remediation of heavy metal(loid)s.

Herein, the study synthesised Fe-Zn-Al layered double hydroxide (LDH) to simultaneously adsorb Cd and Pb from surface and groundwater. The adsorbent was synthesised using a simple and cost-effective co-precipitation technique. The Fe-Zn-Al LDH was characterised for structural, morphological, and textural properties, as well as surface charge, using SEM-EDS, P-XRD, and Nano-ZS Zetasizer. Afterwards, the adsorption parameters, adsorbent mass and sample pH were optimised using central composite design (CCD). This study investigated the practical application of Fe-Zn-Al LDH in removing Cd and Pb in real water samples.

2. Experimental

2.1. Chemicals and reagents

All chemicals used were analytically pure. Aluminium nitrate nonahydrate ($Al(NO_3)_3{\cdot}9H_2O$, 98 % purity), zinc nitrate hexahydrate ($Zn(NO_3)_2{\cdot}6H_2O$, 98 % purity), iron nitrate nonahydrate ($Fe(NO_3)_3{\cdot}9H_2O$, 98 %), sodium carbonate (Na_2CO_3, 99 % purity), sodium hydroxide (NaOH, 99 %) were purchased from Sigma Aldrich. Hydrochloric acid 37 %, ammonia (NH_3), 1 % Nitric acid (HNO_3), 1000 ppm lead (Pb) and cadmium (Cd) were also purchased from Merck (Johannesburg, South Africa), and ultrapure water was mostly used as a solvent.

2.2. Synthesis of Fe-Zn-Al LDH

Fe-Zn-Al LDH was prepared via the co-precipitation synthetic method. Briefly, $Fe(NO_3)_3{\cdot}9H_2O$ (2.33 g), $Zn(NO_3)_2{\cdot}6H_2O$ (3.40 g), and $Al(NO_3)_3{\cdot}9H_2O$ (1.70 g) were dissolved in 80 mL of ultrapure water. A 3 mol alkaline solution was prepared in a separate beaker by dissolving Na_2CO_3 (7.95 g) in 25 mL ultrapure water. The alkaline solution was added dropwise into a stirring solution of mixed metals; the pH of the mixture was adjusted to 9 with 0.1 M NaOH. The solution mixture was then left to age while stirring for 18 hrs at 80 °C under reflux. The resulting Fe-Zn-Al LDH brown precipitates were filtered and washed with excess ultrapure water (100 mL) to remove any unreacted starting materials and dried in an oven at 80 °C for 24 hrs.

2.3. Instrumentation

The synthesised materials were dried using a Labotec EcoTherm oven. The functional groups of the synthesised Fe-Zn-Al LDH were confirmed using Fourier transform infrared (FTIR) spectroscopy (Waltham, MA, USA). The samples were scanned within the wavenumber range of 4000–400 $cm^{-1,}$ and for analysis, KBr was mixed with the sample in the ratio 1:10 to make a pellet. Thereafter, the prepared KBr pellet was placed into the instrument for analysis. This study used a Philips X-ray generator model PW 3710/31 X-ray diffraction XRD, a diffractometer with an automatic sample changer model PW 1775 for the composition and crystallinity of materials. The instrument was using Cu-Kα X-ray ($\lambda = 1.54060$ Å), recording at 2θ range, 2–90°, and operating at a scan speed of 66.045 s. The elemental composition and morphology of Fe-Zn-Al LDH were studied with the transmission electron microscope (TEM) (JEM 2100, JEOL Co. Japan) with an operation voltage of 200Kv and scanning electron microscope (SEM) (TESCAN VEGA 3 xmu, LMH of Czech Republic) in tandem with energy dispersive X-ray spectroscopy (EDX). To analyse the surface charge of the synthesised materials, 30 mg of sample material was suspended in 500 mL ultrapure water. Then, the pH was adjusted with diluted HCl and NaOH solutions in the range of 2–12. After the pH was adjusted, samples were sonicated for 1 hr at room temperature (25 °C) and then analysed using a Nano-ZS Zetasizer (Malvern Instruments, Malvern, UK). The pH was measured using a Bante 901 Benchtop pH meter. The textural properties of Fe-Zn-Al LDH were determined via the CO_2 and N_2 adsorption-desorption analysis. Anton Paar BET surface area analyser (Nova 800) fitted with 21 CFR Part 11-compliant software was utilised for the gas adsorption analysis. The BET surface area was calculated using the Brunauer-Emmett-Teller (BET) equation. The mesopore sizes were estimated using the Barrett-Joyner-Halenda method (BJH) from N_2 adsorption-desorption analysis. On the other hand, the micropore sizes were determined using non-local density functional theory (NLDFT) from CO_2 adsorption-desorption analysis. The ultrasonication was achieved using a SciTech ultrasonic bath system with 50 Hz frequency and 150 W power (Labotec, Midrand, South Africa). The concentration of the analytes was analysed with inductively coupled plasma-optical emission spectrometry (ICP-OES) (iCAP 6500 Duo, Thermo Scientific) coupled with a charge injection device (CID) detector.

2.4. Batch adsorption experiment

The adsorption efficiency of Fe-Zn-Al LDH was assessed by following batch adsorption. Standard solution (1000 mg/L) was used to prepare working solutions, which were diluted with ultrapure water to the required concentration of 1 mg/L, and the calibration standards (0.5 −55 mg/L) were diluted with prepared 1 % nitric acid. The solution pH was adjusted to the required values (4.7–8.3) with 0.1 mol/L hydrochloric acid (HCl) and 1 mol/L ammonia solution. An appropriate amount (11.6–108.4 mg) of Fe-Zn-Al LDH was added to a 50 mL centrifuge tube, followed by a 20 mL solution of Cd and Pb. The sample mixture was sonicated for 30 min to facilitate adsorption, and then, the solution was filtered with a 0.22 μm PVDF filter. Thereafter, the filtered solution was injected into an ICP-OES to determine how much Cd and Pb concentrations were removed from the sample solution.

2.5. Optimisation of batch adsorption

The optimisation of adsorption parameters is important to maximise the adsorption performance of Fe-Zn-Al LDH towards Cd and Pb. Central composite design (CCD) was utilised to achieve optimisation, in which the solution pH and mass of Fe-Zn-Al LDH were varied, ranging from 4.7–8.3 and 11.6–108.4 mg, respectively. The adsorption experiments and analysis were conducted similarly as described in Section 2.4. The

optimum conditions were used to determine removal efficiency (%RE) and adsorption capacity (q_e) of the adsorbent using Eqs. (1) and (2) below, respectively:

$$\%RE = \frac{(C_0 - C_e)}{C_0} \times 100\% \quad (1)$$

$$q_e \frac{(C_0 - C_e)V}{m} \quad (2)$$

In which C_0, C_e, V, and m, are initial concentration, equilibrium concentration, sample volume, and adsorbent mass, respectively.

2.6. Adsorption isotherm studies

The effect of initial concentration in the adsorption process of Cd and Pb by Fe-Zn-Al LDH was investigated via batch adsorption, similar to the method described in Section 2.4. Here, the initial concentrations in a range of 1.0–50 mg/L were prepared in 100 mL solution, and the pH was adjusted to 6.5 and transferred to 250 mL bottles containing 40 mg of Fe-Zn-Al LDH for adsorption. The adsorption data were fitted into two isotherm models, Langmuir and Freundlich, to understand the mode of interaction between Fe-Zn-Al LDH and target analytes.

Langmuir isotherm model:

$$q_e = \frac{q_{max} K_L C_e}{1 + K_L C_e} q_e \quad (3)$$

Where q_e (mg/g) is the adsorption capacity at equilibrium, q_{max} (mg/g) is the maximum adsorption capacity, C_e (mg/L) is the concentration of Cd and Pb at the equilibrium, K_L is the isotherm constant representing the adsorbent affinity to the adsorbate. The latter can be used to calculate the separation factor (R_L) using Eq. (4), which determines if the adsorption was favoured or not.

$$R_L = \frac{1}{1 + K_L C_i} R_L \quad (4)$$

Freundlich isotherm model:

$$q_e = K_F C_e^{1/n} q_e \quad (5)$$

Where q_e (mg/g), K_F, and C_e are the amount of adsorbed Cd and Pb per given mass of Fe-Zn-Al LDH, the coefficient of the Freundlich constant, adsorption intensity and equilibrium concentration of Cd and Pb.

2.7. Adsorption kinetics

This study conducted a batch adsorption and varied contact times to understand its effect on the adsorption of Cd and Pb by Fe-Zn-Al LDH. The experimental conditions, that is, sample volume, pH and adsorbent mass were the same as in Section 2.6, except for sample concentration which was 50 mg/L. The mixtures were ultrasonicated at varying contact times with a range of 5.0–60 min. Thereafter, the supernatants from these experiments were filtered with a 0.22 μm PVDF filter and analysed with ICP-OES for quantification. To understand the adsorption mechanism, the kinetic data was fitted into nonlinear kinetic models including pseudo-first order, pseudo-second order, Elovich, and intra-particle diffusion, using the Eqs. (6)-(9), respectively:

Pseudo first order:

$$q_t = q_e\left(1 - expt^{k_1 t}\right) \quad (6)$$

Pseudo second order:

$$q_t = \frac{k_2 q_e^2}{1 + k_2 q_e t} \quad (7)$$

Elovich model:

$$q_t = \frac{1}{\beta} \ln\left(\alpha\beta t + 1\right) \quad (8)$$

Intra-particle diffusion:

$$q_t = k_i t^{1/2} + C \quad (9)$$

Where q_t (mg/g) is the amount of Cd and Pb adsorbed at time t, q_e is the adsorption capacity at equilibrium. The parameters k_1 (min^{-1}), k_i (mg/g. $min^{-1/2}$), and k_2 (g/mg·min) are adsorption rate constant for pseudo first order, intra-particle diffusion, pseudo second order, respectively.β ((g/mg) is the desorption constant, α (mg/g·min) is the initial adsorption rate and C (mg/g) is the constant providing information about the boundary of the layer thickness.

2.8. Application to real water samples

Surface water and groundwater (borehole denoted as tap) samples were collected from five different sites in King Sabatha Dalidyebo Local Municipality, Eastern Cape, namely Eluxolweni tap (ELX-T) water, Eluxolweni dam (ELX-D), Emavundleni dam (EMD-D), Emavundleni stream (EMD-ST), and Gubevu stream (GBV-ST). They were then transported and stored in the fridge at 4 °C before use. The concentrations of Cd and Pb in real water samples were present in trace levels. Therefore, to assess the feasibility and applicability of Fe-Zn-Al LDH in real applications, the water samples were spiked with 1.0 mg/L of Cd and Pb. Spiking water samples with high concentrations was done to represent water that is highly contaminated by Pb and Cd. A volume of 20 mL of spiked water samples was transferred into 50 mL centrifuge tubes with 40 mg Fe-Zn-Al LDH and then sonicated for 30 min to facilitate adsorption. After that, the liquid solution was filtered with a 0.22 μm PVDF filter before analysis with ICP-OES.

3. Results and discussion

3.1. Functional groups and crystallinity of Fe-Zn-Al LDH

The FTIR spectrum presented in Fig. 1(a) shows the functional groups of Fe-Zn-Al LDH. The broad peak located at 3446 cm^{-1} is for the O—H stretching vibration found on the layered sheets of LDH, and this agrees with the observation of (Tian et al., 2020). The strong narrow band at 1636 cm^{-1} emanates from a stretching vibration of H—O-H, which is attributed to the presence of water molecules and the peak at 1511 cm^{-1} confirmed that carbonate is intercalated in the interlayer spacing of the LDH. These observations are consistent with the characterisation in (Pastor et al., 2020). The 1434 cm^{-1} and 1386 cm^{-1} bands are an asymmetric stretching band of N—O, the nitro compound, which is attributed to the nitrate anion (NO_3^-) of the metal salts (Huang et al., 2022). The band at 1092 cm^{-1} is ascribed to the C—O stretching vibration emanating from carbonate. The peaks at 473 cm^{-1}, 597 cm^{-1} and 880 cm^{-1} are due to vibration of M-O, M-O-M and M-OH, in this case of Fe-Zn-Al LDH, M represents Fe, Zn and Al (Wang et al., 2022; Chubar et al., 2017). The functional groups reported here would aid in facilitating the removal of targeted analytes either by Brøsted-Lewis base site with MO—OH on the surface of the Fe-Zn-Al LDH or by hydrogen bonding and complexation. These adsorptive mechanisms are discussed in detail in Section 3.2.5.

The X-ray diffractogram shown in Fig. 1(b) reveals the diffraction peaks at 2θ = 11.6°, 26°, 33°, 30.3°, 35.7°, 62° and 63° which corresponds to (003), (006), (009), (015), (018), (110) and (113) diffraction planes, respectively. The peaks at 11.6° (003), 26° (006) and 33° (009) are characteristics of hydrotalcite-like LDH materials (Lu et al., 2021) for any LDH framework containing divalent and trivalent metals and the other peaks are ascribed to the Fe-Zn-Al LDH composition. The basal interplanar spacing was 0.71 nm, which was calculated from the (003) diffraction plane by using Bragg's law (nλ = 2dsinθ). The sharp and

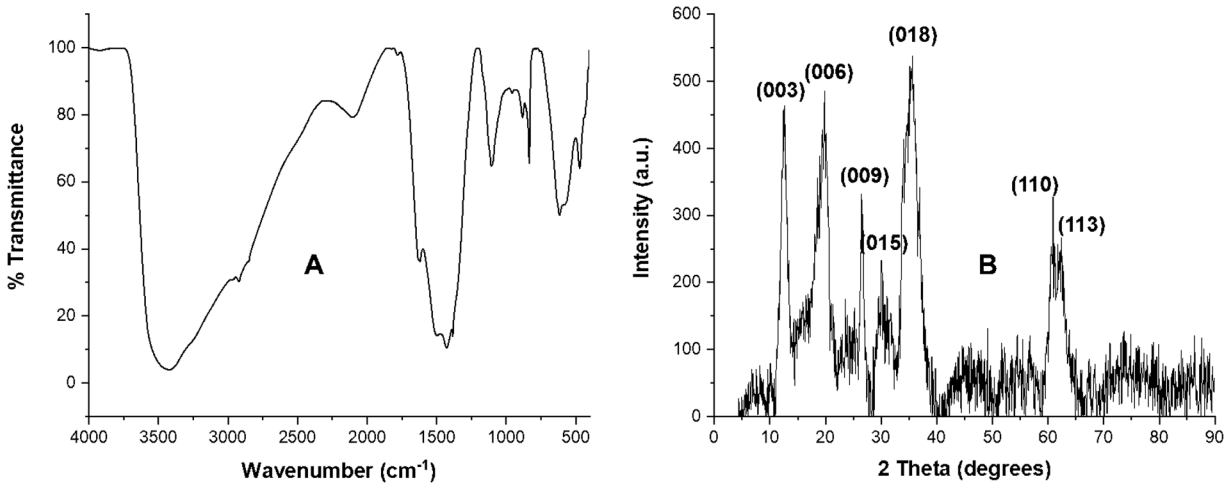

Fig. 1. (a) Fourier transform infrared spectrum and (b) the X-ray diffractogram for Fe-Zn-Al LDH.

intense peaks show that the material is of high crystallinity. The size of the interplanar spacing is big enough, which can be advantageous for the interlayer complexation of the analytes of interest (Cd and Pb) during adsorption.

3.1.1. Elemental composition and morphology of Fe-Zn-Al LDH

Fig. 2 (a & b) represents the SEM image of Fe-Zn-Al LDH and EDS spectrum obtained by analysing the region shown in Fig. 2(a). The synthesised Fe-Zn-Al LDH exhibits Fe, Zn, Al and O elements, which are consistent with the functional groups M-O and M-O-M (with M = Fe, Zn and Al) confirmed by FTIR (Fig. 1(a)). The TEM images in Fig. 2(c) reveal the particles of Fe-Zn-Al LDH, which are agglomerated with platelet-like structures, which agrees with the structure reported by (Xie et al., 2021).

3.1.2. Textural properties and point of zero charge

The surface area, pore diameter, and pore volume of Fe-Zn-Al LDH were evaluated using CO_2 and nitrogen adsorption-desorption analysis. The N_2 adsorption-desorption isotherm presented in Fig. 3(a) shows that the material has a type IV(a) isotherm, which is typical for a material possessing mesopores (Thommes et al., 2015). This was also supported by the presence of an H2(b) hysteresis loop, which is due to the mesoporous structure. Notably, there is a micropore filling at a relative pressure below 0.1, indicating the presence of micropores. This assertion was supported by the pore size distribution, which revealed micropores with sizes 0.35 nm, 0.55 nm and 0.79 nm, Fig. 3(b).

On the other hand, BJH pore size distribution shows peaks at 3.74 nm and 11.0 nm in the mesoporous range, authenticating the average sizes of the mesopores, Fig. 3(c). The synergistic effect of the micropores and mesopores may enhance the adsorption process of Fe-Zn-Al LDH, in which mesopores might increase the diffusion of metal species and micropores accommodate the adsorbed metal species (Wei et al., 2023). Fe-Zn-Al LDH has a large BET surface area and pore volume, which were 171 m^2/g and 0.31 cm^3/g, respectively, suggesting the material exhibits large active sorptive sites for targeted analytes.

Fig. 3(d) represents the zeta potential of Fe-Zn-Al LDH, which was measured at different pH values ranging from 2–12, which is necessary to understand the surface charge. The isoelectric point, also referred to as the point of zero charge (pH_{PZC}), was 9.2, and here, the surface charge density is neutral, and the zeta potential of the material is zero (Li et al., 2020). It can be observed from Fig. 3(d) that the Fe-Zn-Al LDH surface becomes positively charged at pH below 9.2 and negatively charged above 9.2. Above the pH of 9.2, the surface of the material will favour the attractive adsorption of cationic analytes by mode of electrostatic attraction and below the pH of 9.2, the mode of adsorption will be by surface complexation, ion exchange and other possible mechanisms, which will be explained in detail in sections below.

3.2. Evaluation of batch adsorption of metals (Cd and Pb) with Fe-Zn-Al LDH as adsorbent

3.2.1. Optimisation of the batch removal process

Here, the factors influencing the removal of Cd and Pb with Fe-Zn-Al LDH were optimised with CCD; here, two independent parameters, the

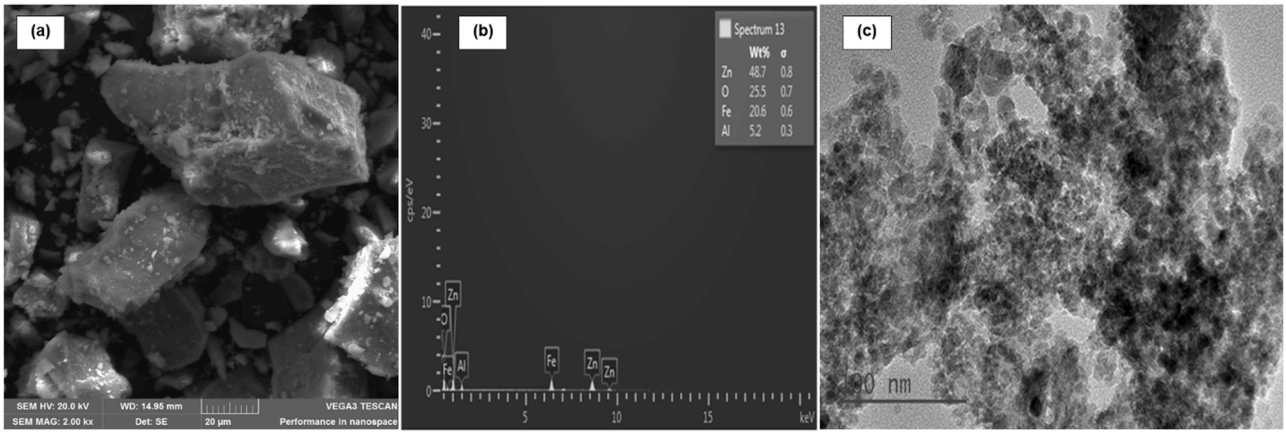

Fig. 2. (a) Scanning electron microscope image, (b) Energy dispersive X-ray spectroscopy and (c) transmission electron microscope image of Fe-Zn-Al LDH.

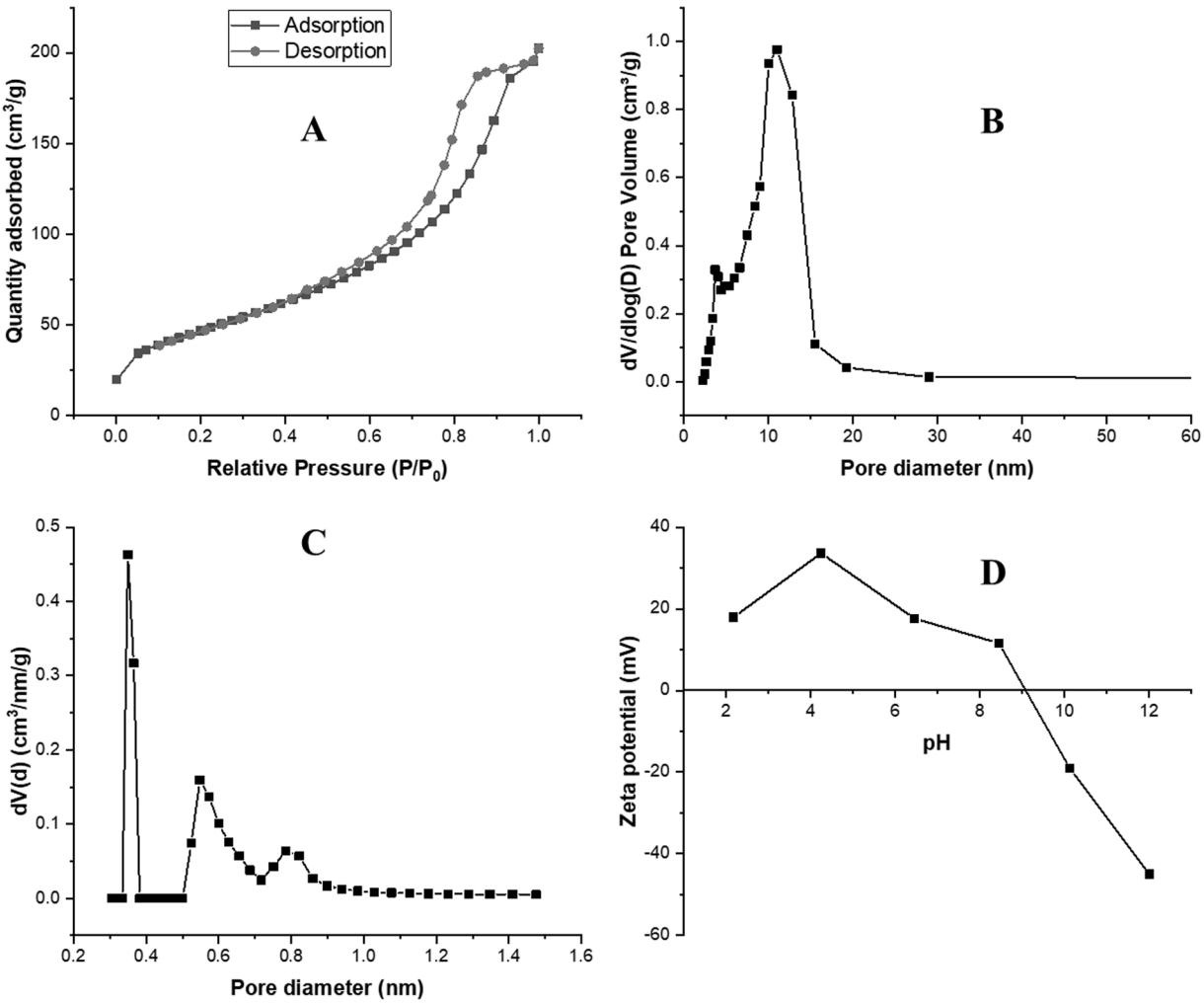

Fig. 3. (a) N_2 adsorption-desorption isotherm, (b) BJH pore size distribution (desorption branch) determined using N_2 adsorption-desorption, (c) pore size distribution determined using CO_2 adsorption, and (d) zeta potential for Fe-Zn-Al LDH.

mass of the adsorbent (MA) and solution pH, were assessed to enhance the adsorption process. The CCD matrix exhibiting 12 experiments and the response with respect to Cd are presented in Table 1. The data in Table 1 were then used for the analysis of variance (ANOVA), which reproduced the Pareto chart, surface plot, predicted values, and desirability. In the Pareto chart Fig. 4(a), the length of the bars corresponds with the effect of each assessed parameter on the removal process and how they interact. At the same time, the vertical lines show a significant influence at a 95 % confidence level. The parameters are said to be substantial when the bar representing each parameter passes the line ($p = 0.05$) (Nyaba et al., 2016). The results show that pH and MA are all significant at the 95 % confidence level, which means the adsorptive removal of Cd with Fe-Zn-Al LDH was influenced by all the investigated variables.

Table 1
The Central composite design with % removal efficiency.

Standard Run	pH	MA(mg)	Cd %RE
1	5	20	48.0 ± 2.3
2	5	100	76.7 ± 3.1
3	8	20	68.8 ± 3.2
4	8	100	87.9 ± 3.3
5	4.7	60	75.3 ± 2.8
6	8.3	60	85.5 ± 2.7
7	6.5	11.6	53.2 ± 2.9
8	6.5	108.4	78.6 ± 2.9
9 (C)	6.5	60	73.7 ± 3.2
10 (C)	6.5	60	71.6 ± 2.6
11 (C)	6.5	60	71.2 ± 2.7
12 (C)	6.5	60	70.7 ± 3.1

The analytical response with assessed variables was used to obtain the response surface plot, which is represented in Fig. 4(b). The response surface plot has been used to show the interaction of independent variables (Li et al., 2020). The increase in %RE with mass is because the mass of Fe-Zn-Al LDH increases with the number of active sorptive sites available to bind and accommodate Cd. At the low pH values, the surface of Fe-Zn-Al LDH is positively charged, and Cd is also positively charged, which results in the lower adsorption of Cd. Still, the increase in the solution pH showed a positive impact on the uptake of Cd. The pH analysis was conducted up to the pH value of 8, which is below the point of zero charge of Fe-Zn-Al LDH observed in Fig. 4(b). The increase in the removal of Cd might be due to cation exchange, where Cd undergoes ion exchange with one of the metals on the Fe-Zn-Al LDH, and by interlayer complexation with the CO_3^{2-} on the interlayer spacing. Another possible mechanism is through surface complexation with Brøsted-Lewis base site of MO—OH on the surface of the Fe-Zn-Al LDH, thus making pH to have influence on the surface charge of the adsorbent which might enhance analytes uptake.

The desirability function was applied to optimise independent variables simultaneously, and the functions are used to convert the anticipated responses into a dimensionless desirability value. Fig. 5(c) was used to optimise the investigated variables. As shown, the desirability

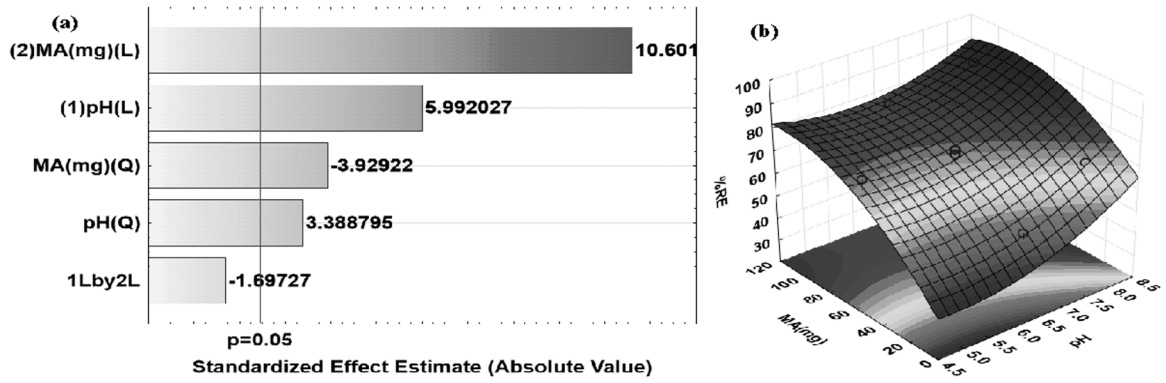

Fig. 4. (a) Pareto chart of standardised effects and (b) 3D response surface plot for the removal of Cd using Fe-Zn-Al LDH.

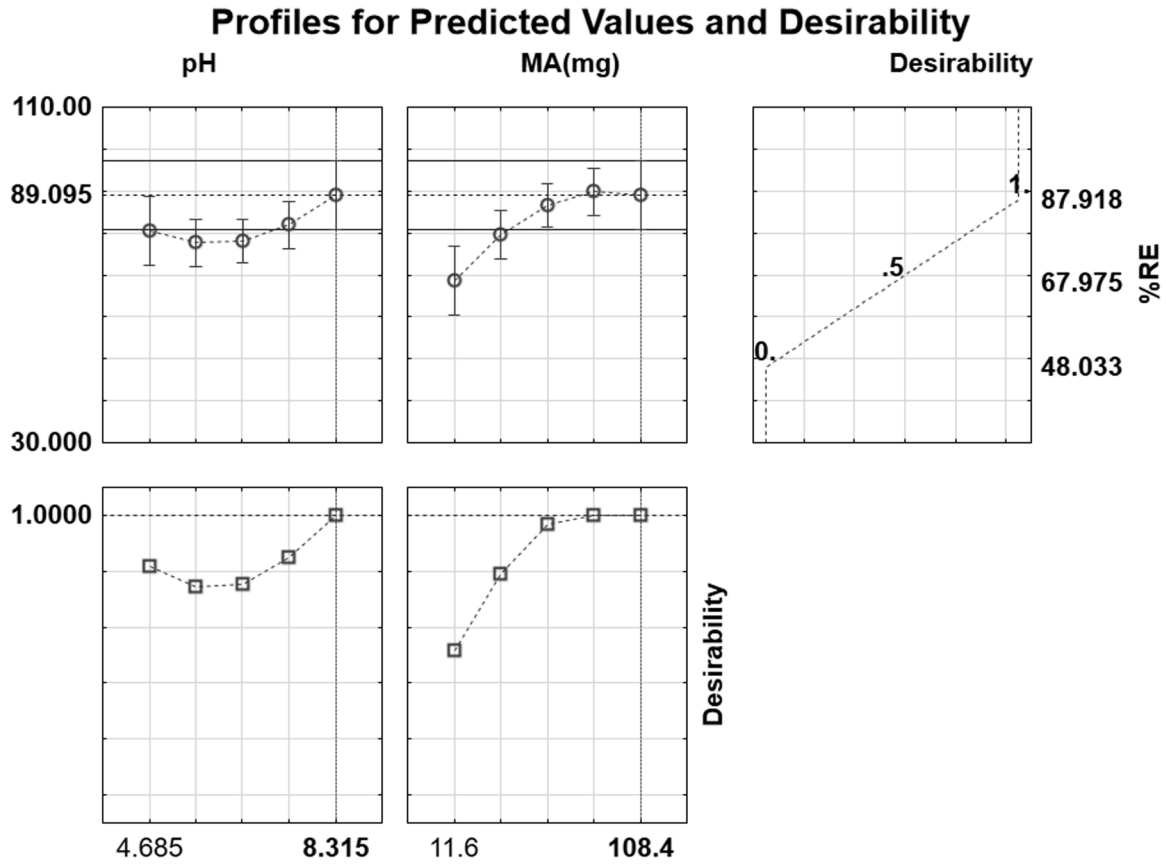

Fig. 5. Desirability profile for the optimisation of experimental parameters affecting the adsorptive removal of Cd and Pb using Fe-Zn-Al LDH.

values ranged from 0–1, where $D = 0$ is the minimum desirability value, 0.5 is the central point, and $D = 1$ is the maximum desirability value and the most desirable value with a %RE of 87.9 %. The maximum desirability value was utilised to obtain the optimum sample pH and MA. From the results in Fig. 5, it can be observed that the optimum conditions for Fe-Zn-Al LDH during the adsorptive removal of Cd are a pH of 8.4 and an MA of 108 mg. The plot shows that even 40 mg is within the maximum desirability value. Furthermore, to avoid precipitation of trace metals, a pH of 6.5 was used. Therefore, based on the cost-effectiveness and environmental relevance, 40 mg of Fe-Zn-Al LDH adsorbent and a sample pH of 6.5 were regarded as the optimum conditions. These optimum conditions were confirmed experimentally, and the removal efficiencies were found to be 94.6 % and 97.8 % for Cd and Pb, respectively.

3.2.2. *Adsorption isotherm*

The relationship between Fe-Zn-Al LDH and Cd and Pb can be better understood using isotherms. The form of isotherms is determined by several variables, including the metal ion concentration in the solution, the respective adsorbing capacities of the metal ions, and the level of competition of the metal ions to bind to the active sites of the adsorbent (Mashile et al., 2018). The experimental data for the adsorption of Cd and Pb were fitted into the nonlinear Freundlich isotherm and Langmuir isotherm models, as shown in Figures S1 and S2. The Langmuir model is predicated on the idea of adsorption homogeneity, which includes the accessibility of the adsorptive monolayer active sites for binding, uniform adsorption energy without metal ion transmigration on the plane of the adsorbent surface, and no interaction among the adsorbed metal ions. The separation factor, $R_{L,}$ determines the favourability of the model. When $R_L > 1$, it means the adsorption process is unfavoured, $R_L =$

0 mean the process is irreversible and when $0<R_L>1$ means the adsorption process is favourable. In contrast, the Freundlich model is predicated on the idea of multilayer adsorption, with lateral interactions among species that are adsorbed on the heterogeneous adsorbent surface. Values of n or 1/n are temperature-dependent, and they represent adsorption parameters like surface heterogeneity. The process of adsorption is favoured when $1/n > 0$, and unfavoured when $1/n > 1$ and irreversible for $1/n = 1$ (Manirethan et al., 2018; Dutta et al., 2016). Table 2 represents the summary of the outcomes of fitting the Freundlich and Langmuir models in the adsorption of Cd and Pb by Fe-Zn-Al LDH. The results showed that the data is explained by both the Langmuir and the Freundlich models, suggesting the presence of monolayer and multilayer adsorption behaviour occurred during the sorption process of Cd and Pb (Zhang et al., 2022). However, the Freundlich isotherm model fitted better than the Langmuir model, suggesting that the Fe-Zn-Al LDH surface active sites were distributed heterogeneously. Furthermore, based on the values of n (Freundlich intensity parameter) from Table 2, the 1/n values are 0.25 and 0.71 for Cd and Pd, respectively, which indicates that the adsorption of Cd and Pb is highly favoured and has high affinity for Fe-Zn-Al LDH adsorbent.

3.2.3. Adsorption kinetics

The effect of time on the adsorptive removal of Cd and Pb with Fe-Zn-Al LDH was studied by varying time in the range of 5.0–60 min, and the other optimum experimental parameters were kept constant. The kinetic data were modelled into four kinetic models: pseudo-first order, pseudo-second order, Elovich model and intra-particle diffusion, as shown in Figures S3–6, to understand the rate-determining step and mechanism of the removal of Cd and Pb. The summary of the kinetic model parameters is represented in Table 3. It can be observed that the data for the adsorption of Cd and Pb best fitted the pseudo-second order and Elovich model, suggesting that the adsorption process is dominated by chemisorption with physisorption playing a secondary role (Deng et al., 2025). However, according to the results in Table 3, correlation coefficients for the Elovich model were higher than those of the other models, and this suggests that the removal of both Cd and Pb was dominated by a chemisorption process with a heterogeneous surface. The fitting of the pseudo-second order model suggests that chemisorption involves the sharing of electrons or ion exchange between adsorbents and metal ions (N. Zhang et al., 2023). The Elovich kinetic model agreed with the Freundlich model. Intraparticle diffusion was used to state the rate-determining stage, and from the data, it was observed that the adsorption of Cd and Pb occurred in two stages. Furthermore, the intraparticle diffusion graph did not begin at the origin, suggesting that boundary layer diffusion played a role in the Cd and Pb adsorption process as well. From this, it was confirmed that the adsorption of Cd and Pb occurred by the first boundary layer and then the intraparticle diffusion on the pores of the Fe-Zn-Al LDH. By using the values of C, which indicates boundary layer thickness (a big value of C shows that the boundary layer has more effect) (Saini and Melo, 2013). Table 3 indicates substantially higher C_2 values (19.4 mg/g for Cd and 124 mg/g for Pb) in the second step compared to the C_1 (7.44 mg/g for Cd and 120 mg/g for Pb) in the first step. This confirms that the adsorption removal of both Pb and Cd is determined by intraparticle diffusion.

3.2.4. Possible adsorption mechanism

The plausible adsorption mechanism between the Fe-Zn-Al LDH and the target analytes (Cd and Pb) is chemisorption on a heterogeneous surface, based on the information obtained from the isotherm and kinetic models. The mechanism involved the electrostatic attraction between the CO_3^{2-} and NO_3^- on the Fe-Zn-Al LDH surface and trace metal cations. Furthermore, trace metal cations could be bonded to free hydroxyl and deprotonated hydroxyl groups on the surface of Fe-Zn-Al LDH, thus resulting in surface complexation (López-Luna et al., 2019). The coordination of the Cd and Pb via the OH groups replacing hydrogen is substantiated by the significant increase in intensity (relative to other peaks) and wavenumber (compared to peaks in pure LDH) of the peak at 455 cm^{-1} associated with M-O and disappearance of the OH functional group peaks, thus indicating complexation via the oxygen of OH group. The interaction of Cd and Pb ions with some anions, such as (OH^- and CO_3^{2-}) released from the surface of Fe-Zn-Al LDH leads to the formation of mineral precipitates such as ($Cd(OH)_2$) and $Pb_3(CO_3)_2(OH)_2$, thus leading to another adsorption mechanism called mineral precipitation (Hossain et al., 2022). This phenomenon was confirmed by the disappearance of the FTIR peaks attributed to OH and CO_3 functional groups after adsorption, which were present in the FTIR spectrum of pure LDH (Fig. 1(a) and Fig. 6(a)). The X-ray diffractogram (Fig. 6(b)) of Fe-Zn-Al LDH post adsorption of Cd and Pb showed new peaks in the range of 20–30°, which were not present in the pure LDH. The peaks are attributed to the $Pb_3(CO_3)_2(OH)_2$ and $CdCO_3$, which confirms the successful coordination and precipitation of Cd and Pb (Zhang et al., 2021). Therefore, it could be concluded that the overall adsorption mechanism included precipitation reaction, chelation or electrostatic attraction and surface complexation, and these findings are consistent with the literature (Sun et al., 2022; Trujillano et al., 2023). The successful adsorption of Cd and Pb onto Fe-Zn-Al LDH was further substantiated by SEM, EDS, and mapping (Fig. 6 (c and d)), which showed the presence of Cd and Pb.

3.2.5. Comparison with previous studies

The performance of Fe-Zn-Al LDH in removing Cd and Pb was evaluated in terms of adsorption capacity, and the results were compared with those of other LDH-based adsorbents. The comparison was based on the experimental conditions, and the results are presented in Table 4. Based on the adsorption capacities, Fe-Zn-Al LDH showed high adsorptive removal for Pb compared to most studies. On the other hand, Cd was poorly removed by Fe-Zn-Al LDH compared to most studies, although most studies modified LDH to enhance their active adsorptive sites. The performances of functionalised LDHs were comparable and, in some cases, poorer compared to our pristine LDH, despite requiring multiple steps for synthesis, which increases their synthesis costs. Therefore, the advantage of Fe-Zn-Al LDH material is that it does not need cumbersome modification steps, and they are cost-effective, thus making it preferable for the removal of Cd and Pb. For instance, a different study prepared MgAl-LDH@AC nanocomposites for

Table 2
The summary of the Freundlich model and Langmuir model applied for the adsorption process of Cd and Pb with Fe-Zn-Al LDH.

Metals	Freundlich isotherm model			Langmuir isotherm model		
	K_F(mg/g)	1/n	R^2	q_{max}(mg/g)	K_L(L/mg)	R^2
Cd	4.46	0.25	0.925	11.9	0.25	0.916
Pb	264	0.71	0.996	280	2.26	0.988

Table 3
The summary of kinetic models with their parameters for the adsorption of Cd and Pb with Fe-Zn-Al LDH adsorbent.

Models	Parameters	Cd	Pb
Pseudo first order	q_e	23.5	123
	k_1	0.151	0.824
	R^2	0.860	0.245
Pseudo second order	q_e	25.8	124
	k_2	0.0097	0.053
	R^2	0.938	0.632
Elovich model	α	52.5	9.077
	β	0.27	0.581
	R^2	0.966	0.790
Intra-particle diffusion	$K_{i(1)}$	3.2	0.36
	$K_{i(2)}$	0.66	0.063
	C_1	7.44	120
	C_2	19.4	124
	$R^2_{(1}$	0.967	0.885
	$R^2_{(2)}$	0.835	0.817

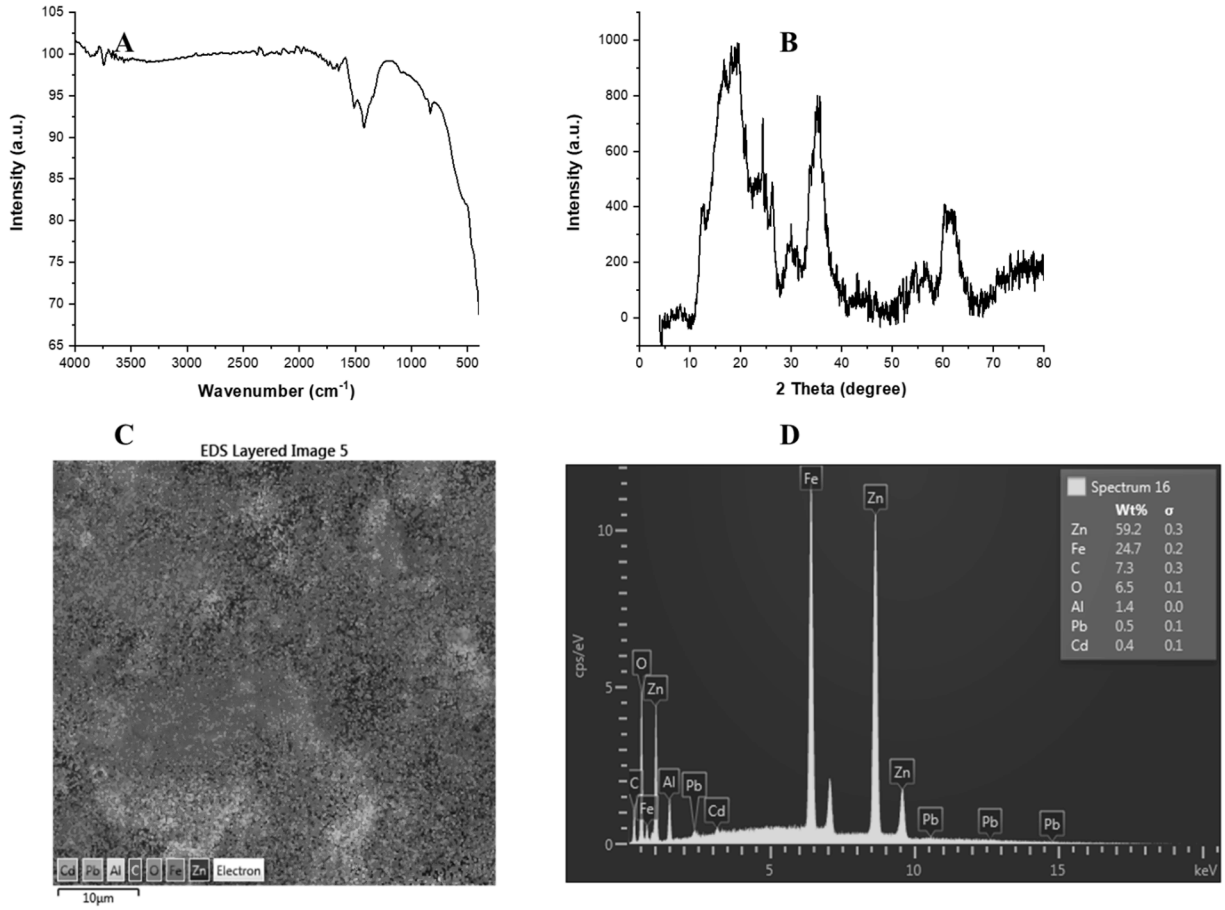

Fig. 6. (a) FTIR spectrum and (b) X-ray diffractogram, (c) SEM-mapping, and (d) energy dispersive X-ray spectroscopy for Fe-Zn-Al LDH after adsorption of Cd and Pb.

Table 4
Adsorption capacities for Cd and Pb by LDH-based adsorbents reported in the literature.

Adsorbents	Experimental conditions				Adsorption capacity (mg/g)		Refs
	pH	Dosage (g/L)	Contact time (min)	Initial conc. (mg/L)	Cd	Pb	
Mg/Al LDH-SHMP	5.0	5.0	120	25–800	24.3	45.7	(Hossain et al., 2022)
MgAl-LDH-200	5–7	1.5	240	20–1000	126	69.1	(Song et al., 2023)
MgAl-LDH-4000	5–7	1.5	240	20–1000	102	61.3	(Song et al., 2023)
MgAl-LDH	3–4	10	60	30–200	7.88	12.6	(Mo et al., 2024)
CaAl-LDH	5	0.5	20	10–500	437	786	(Hou et al., 2024)
MgAl-LDH@AC	5	1	420	50–300	-	94.6	(Khalil et al., 2023)
ZnMgAl LDH/RHB	6	0.4	15	5–100		124	(Shafiq et al., 2023)
20EDTMP-Mg/Al LDH	6.5	1	60	25–500	161	249	(Li et al., 2023)
FeMnNi-LTH	5.5	1	240	-	56.9	254	(Zhou et al., 2024)
Ag@Zn-Al LDH	8	-	80	-	402	538	(Asha et al., 2023)
MgAl-LDH	6	1	75–140	10–1000	36.8	30.2	(Wang et al., 2021)
MgAl-LDH/Cys	6	1	75–140	10–1000	136	280	(Wang et al., 2022)
Fe-Zn-Al LDH	6.58	0.4	30	1–50	11.6	280	This study

MgAl-LDH-200 and 4000: MgAl-LDH modified with polyethylene glycol with molecular weight of 200 and 4000; SHMP: sodium hexametaphosphate; 20EDTMP: 20 % Ethylenediamine-tetramethylene phosphonic acid; LTH: layered triple hydroxide.

the removal of Pb; this study used more than two times the adsorbent dosage and needed eight times more contact time to achieve about three times less adsorption capacity compared to Fe-Zn-Al LDH (Table 4) (Khalil et al., 2023). Another study combined LDH with sodium hexametaphosphate (SHMP) to increase the active adsorption sites to accommodate Cd and Pb (Hossain et al., 2022). When compared to our pristine LDH, their adsorbent employed more adsorbent dosage (12.5 times more) and longer contact time (4 times more) yet performed poorly compared to the LDH prepared in this study, Table 4. This vouches for the high removal performance and cost effectiveness of unfunctionalsed LDH.

3.3. Evaluation of the adsorption efficiency of Fe-Zn-Al LDH for the removal of Cd and Pb in real water

The adsorptive performance of Fe-Zn-Al LDH towards Cd and Pb in complex real water samples was investigated. The concentration of Cd and Pb in water samples 0.5–3.8 µg/L and 9.3–28.5 µg/L, respectively. It is important to note that the investigated water samples were characterised by high concentrations of major cations and high turbidity. The

adsorbent was applied directly with spiking, and 100 % removal efficiency was achieved. The samples were spiked to investigate the removal efficiency at high concentrations of Cd and Pb in the presence of coexisting ions. The results represented in Table 5 show that Pb and Cd had higher % RE when considering the possibility of competition for active sites in the complex water sample. Pb ions have a greater affinity for the oxygen groups of the abundant hydroxyl groups of LDH than Cd and other heavy metals in water (Xue et al., 2009). This may be the reason for a higher %RE for Pb than Cd in most sites, where there is competition for adsorptive sites, and Pb coordinates with these hydroxyl groups faster due to high affinity. Notably, in real water, the adsorption performance of Fe-Zn-Al LDH towards Pb and Cd is largely different from that in simulated water. This phenomenon may be ascribed to the competition for ionic exchangeability of the analytes, which is facilitated by ionic radius. The ionic radius of Pb ions and other common heavy metals in water is greater than that of Cd ions. As a result, Cd) may more easily fit into the Fe-Zn-Al LDH -LDL interlayer gaps because of its smaller size, which may also result in more advantageous ion exchange processes (X. Zhang et al., 2023), whereas Pb ions are competing with various heavy metals for the other adsorptive sites. In water samples, there are various ions such as cations, organics and others that might co-exist in the water, which can compete for the binding site with the analytes of interest, which might be the main reason for the reduced % RE in other water samples from sites.

3.4. Regeneration, reusability and safe disposal considerations

The regeneration and reusability of the spent adsorbent are important parameters that evaluate the economic viability and environmental sustainability of the adsorption process (Šoštarić et al., 2018). Therefore, regeneration studies are essential to assess the stability and reusability of the ability of the Fe-Zn-Al LDH adsorbent. The Fe-Zn-Al LDH adsorbent loaded with Cd and Pb was treated with 15 mL of 0.1 M HCl to desorb the metal ions. The adsorbent was then washed three times with 20 mL deionised water, followed by rinsing with ethanol to reduce the amount of water molecules, and then dried at 80 °C for 3 hrs. The spent adsorbent was used for the adsorption of Cd and Pb. The Zn-Al LDH adsorbent could be reused up to three adsorption-desorption cycles without significant loss of its adsorption efficiency (Figure S7). The drastic decrease in the adsorption capacity after the third cycle could be due to the leaching of Fe, Zn and Al from the adsorbent during the desorption step. These findings suggest that the regenerated adsorbent had a low degree of regenerability. Even though the main objective of the study was to assess the adsorption performance of Fe-Zn-Al LDH adsorbent for the removal of Cd and Pb, disposal of spent adsorbent loaded with Cd and Pb is crucial for sustainable wastewater management to prevent secondary pollution (Jyothi et al., 2024; Mushahary et al., 2024). The current adsorbent has a limited degree of regeneration; therefore, safe disposal could include encapsulating the Fe-Zn-Al LDH adsorbent loaded with Cd and Pb in cement matrices to prevent leaching of trace metals into the environment. Furthermore, the heady metal-loaded adsorbent could be solidified or stabilised to stable metal oxides before disposal into landfills (Jyothi et al., 2024; Mushahary et al., 2024).

Table 5
The % removal efficiency of Cd and Pb after adsorption with Fe-Zn-Al LDH in water samples from different sites in Eastern Cape Province.

Sampling sites	Cd	Pb
	%Removal efficiency (%RE)	
ELX-T	59.6 ± 3.1	83.0 ± 2.9
ELX-D	51.4 ± 3.2	92.7 ± 2.7
EVD-D	67.8 ± 3.4	77.4 ± 3.1
EVD-ST	55.4 ± 2.9	59.8 ± 3.3
GBV-ST	64.6 ± 3.2	55.7 ± 3.7

Eluxolweni tap (ELX-T) water, Eluxolweni dam (ELX-D), Emavundleni dam (EMD-D), Emavundleni stream (EMD-ST), and Gubevu stream (GBV-ST). Add adsorption conditions.

3.5. Cost estimation of removing Cd and Pb using adsorption technology

Cost assessment of water treatment via adsorption technology is a significant factor that is used to evaluate the real-life applicability and cost-effectiveness of the proposed process. Typically, the cost of the adsorption process depends on the cost of producing the adsorbent and the operational cost of the method (Benjelloun et al., 2024; Shaikh et al., 2022). The current study successfully prepared Fe-Zn-Al LDH adsorbent for the adsorptive removal of Cd and Pb from ground and surface water. The cost estimation for the synthesis of Fe-Zn-Al LDH adsorbent included chemicals and electricity consumption, and the details are presented in Table S1. As shown in Table S1, the estimated lab-scale preparation cost of producing 1 kg of Fe-Zn-Al LDH adsorbent was found to be 2179.26 USD (R38577.78). Under optimum conditions, an Fe-Zn-Al LDH adsorbent dose of 2 g/L was used to achieve the maximum removal of Cd and Pb from water. This implied that 1 kg of Fe-Zn-Al LDH adsorbent could treat approximately 500 L of water contaminated by Cd and Pb to achieve removal efficiencies greater than 85 %. Therefore, the cost of treating surface and groundwater using Fe-Zn-Al LDH adsorbent is estimated to be 4.36 USD/L. Based on the sorption capacities (11.9 mg/g and 280 mg/g for Cd and Pb), the adsorption cost of removing 1 g of Cd and Pb is 183 USD and 7.78 USD for Cd and Pb, respectively. The economic and sustainable production cost of Fe-Zn-Al LDH adsorbent could be lowered by using waste materials that are abundant in South Africa, such as red mud, slag and coal fly ash.

4. Conclusion

The Fe-Zn-Al LDH was effectively synthesised by the co-precipitation method and characterised to confirm the elemental composition, morphology, functional groups, textural properties and crystallinity. From the characterisation, it was confirmed that the material synthesised was LDH with a high specific surface area containing micropores and mesopores. The adsorption performance Fe-Zn-Al LDH adsorbent was evaluated for the removal of heavy metal ions in aqueous solutions and real water samples. The optimum conditions for the adsorption process were obtained using CCD, and they were pH 6.5 and an adsorbent dosage of 2 g/L (40 mg Fe-Zn-Al LDH adsorbent in 20 mL of sample). Furthermore, the experimental results demonstrated that the removal of Cd and Pb increased with increasing adsorbent dose, contact time and initial concentration of the heavy metals. The interaction of Cd and Pb with Fe-Zn-Al LDH was studied by fitting the equilibrium adsorption data into two isotherm models. The slight differences in correlation coefficients of the investigated isotherm models suggested that the adsorption data for uptake of Cd and Pb fitted to both the Freundlich and Langmuir models, suggesting that adsorptive removal of metal ions by Fe-Zn-Al LDH was explained by different adsorption mechanisms. A similar phenomenon was observed during the kinetics studies, where the data fitted the Elovich and pseudo-second-order kinetic models. According to the isotherm, kinetics and mechanism analysis, precipitation reaction, the adsorption pathways were surface complexation or chelation and electrostatic attraction. Furthermore, the Fe-Zn-Al LDH adsorbent exhibited high affinity towards Pb compared to Cd. The Fe-Zn-Al LDH adsorbent maintained acceptable adsorption performance when applied for the removal of Cd and Pb in surface water and groundwater, where many common coexisting ions are present.

Funding information

This study was financially supported by the Department of Science, Technology and Innovation-National Research Foundation South African Research Chair Initiative (DSTI-NRF SARChI) funding instrument, grant no. 91230 and Water Research Commission (WRC), grant no.

C2023-2024-01448.

Declaration of generative AI and AI-assisted technologies in the writing process

During the preparation of this work the author(s) used Grammarly in order to improve English language. After using Grammarly, the author (s) reviewed and edited the content as needed and take(s) full responsibility for the content of the publication.

CRediT authorship contribution statement

Ramatsobane Rosy Phogole: Writing – original draft, Visualization, Validation, Methodology, Investigation, Formal analysis, Data curation, Conceptualization. **Philani Perfect Mpungose:** Writing – review & editing, Visualization, Validation, Supervision, Methodology, Data curation, Conceptualization. **Luthando Nyaba:** Writing – review & editing, Visualization, Validation, Supervision, Methodology, Investigation, Formal analysis, Data curation, Conceptualization. **Mthokozisi Mnguni:** Writing – review & editing, Visualization, Validation, Supervision, Methodology, Investigation, Formal analysis, Data curation, Conceptualization. **Philiswa Nosizo Nomngongo:** Writing – review & editing, Visualization, Validation, Supervision, Software, Resources, Project administration, Methodology, Investigation, Funding acquisition, Formal analysis, Data curation, Conceptualization.

Declaration of competing interest

The authors declare that they have no known competing financial interests or personal relationships that could have appeared to influence the work reported in this paper

Acknowledgements

The authors wish to acknowledge and thank the University of Johannesburg, Faculty of Science, and Department of Chemical Sciences for laboratory space.

Supplementary materials

Supplementary material associated with this article can be found, in the online version, at doi:10.1016/j.hazadv.2025.100876.

Data availability

Data will be made available on request.

References

Abushawish, A., Chatla, A., Almanassra, I.W., Shanableh, A., Atieh, M.A., 2024. Co-Al layered double oxide activated carbon composite for eliminating lead ions from water. J. Phys.: Conf. Ser. 2751 (1), 12008. https://iopscience.iop.org/article/10.1088/1742-6596/2751/1/012008/meta.

Asha, P.K., Deepak, K., Prashanth, M.K., Parashuram, L., Devi, V.A., Archana, S., Raghu, M.S., 2023. Ag decorated Zn-Al layered double hydroxide for adsorptive removal of heavy metals and antimicrobial activity: numerical investigations, statistical analysis and kinetic studies. Environ. Nanotechnol. Monit. Manag. 20, 100787. https://doi.org/10.1016/j.enmm.2023.100787.

Benjelloun, M., Miyah, Y., Ssouni, S., Iaich, S., El-habacha, M., Lagdali, S., Bouslamti, R., 2024. Capparis spinosa L waste activated carbon as an efficient adsorbent for crystal violet toxic dye removal: modeling, optimization by experimental design, and ecological analysis. Chin. J. Chem. Eng. 71, 283–302.

Bordoloi, S., Nath, M., Dutta, R.K., 2013. pH-conditioning for simultaneous removal of arsenic and iron ions from groundwater. Process Saf. Environ. Prot. 91 (5), 405–414. https://doi.org/10.1016/j.psep.2012.10.002.

Chubar, N., Gilmour, R., Gerda, V., Mičušík, M., Omastova, M., Heister, K., Man, P., Fraissard, J., Zaitsev, V., 2017. Layered double hydroxides as the next generation inorganic anion exchangers: synthetic methods versus applicability. Adv. Colloid Interface. Sci. 245, 62–80. https://doi.org/10.1016/j.cis.2017.04.013.

Conterosito, E., Gianotti, V., Boccaleri, E., Palin, L., Milanesio, M., Viterbo, D., 2018. Facile preparation methods of hydrotalcite layered materials and their structural characterisation by combined techniques. Inorg. Chim Acta. 470, 36–50. https://doi.org/10.1016/j.ica.2017.08.007.

Deng, S., Ren, B., Cheng, S., Hou, B., Deng, R., Zhu, G., 2025. Study on the adsorption performance of carbon-magnetic modified sepiolite nanocomposite for Sb (V), Cd (II), Pb (II), and Zn (II): optimal conditions, mechanisms, and practical applications in mining areas. J. Hazard. Mater. 487, 137129. https://doi.org/10.1016/j.jhazmat.2025.137129.

Dutta, A., Diao, Y., Jain, R., Rene, E.R., Dutta, S., 2016. Adsorption of cadmium from aqueous solutions onto coffee grounds and wheat straw: equilibrium and kinetic study. J. Environ. Eng. 142 (9), C4015014. https://doi.org/10.1061/(ASCE)EE.1943-7870.0001015.

Hossain, M.T., Khandaker, S., Bashar, M.M., Islam, A., Ahmed, M., Akter, R., Awual, M. R., 2022. Simultaneous toxic Cd (II) and Pb (II) encapsulation from contaminated water using Mg/Al-LDH composite materials. J. Mol. Liq. 368, 120810. https://doi.org/10.1016/j.molliq.2022.120810.

Hou, J.F., Sun, Q., Hao, X.Z., 2024. Adsorption performance and mechanistic study of Pb, Cd and As by CaAl-LDH in wastewater. J. Cent. South Univ. 31 (4), 1292–1305. https://doi.org/10.1007/s11771-024-5627-2.

Huang, Y., Liu, C., Rad, S., He, H., Qin, L., 2022. A comprehensive review of layered double hydroxide-based carbon composites as an environmental multifunctional material for wastewater treatment. Processes 10 (4), 617. https://doi.org/10.3390/pr10040617.

Jyothi, M.N., Vajitha, G., Gandhi, T.P., Ramaiah, B.J., Maliyekkal, S.M., 2024. Granulated Fe-Mn bimetal-oxides: a reusable adsorbent for mercury removal and valorisation of spent adsorbent as a retarding agent and compressive strength enhancer in cementitious materials. Process Saf. Environ. Prot. 184, 1293–1305.

Karim, A., Raji, Z., Karam, A., Khalloufi, S., 2023. Valorisation of fibrous plant-based food waste as biosorbents for remediation of heavy metals from wastewater—a review. Molecules 28 (10), 4205. https://doi.org/10.3390/molecules28104205.

Khalil, A.K., Almanassra, I.W., Chatla, A., Ihsanullah, I., Laoui, T., Atieh, M.A., 2023. Insights into the adsorption of lead ions by Mg-Al LDH doped activated carbon composites: implications for fixed bed column and batch applications. Chem. Eng. Sci. 281, 119192. https://doi.org/10.1016/j.ces.2023.119192.

Kumar, R., Sharma, P., Rose, P.K., Sahoo, P.K., Bhattacharya, P., Pandey, A., Kumar, M., 2023. Co-transport and deposition of fluoride using rice husk-derived biochar in saturated porous media: effect of solution chemistry and surface properties. Environ. Technol. Innov. 30, 103056. https://doi.org/10.1016/j.eti.2023.103056.

López-Luna, J., Ramírez-Montes, L.E., Martinez-Vargas, S., Martínez, A.I., Mijangos-Ricardez, O.F., González-Chávez, M.D.C.A., Vázquez-Hipólito, V., 2019. Linear and nonlinear kinetic and isotherm adsorption models for arsenic removal by manganese ferrite nanoparticles. SN Appl. Sci. 1, 1–19. https://doi.org/10.1007/s42452-019-0977-3.

Li, A., Deng, H., Ye, C., Jiang, Y., 2020. Fabrication and characterisation of novel znal-layered double hydroxide for the superadsorption of organic contaminants from wastewater. ACS Omega. 5 (25), 15152–15161. https://doi.org/10.1021/acsomega.0c01092.

Li, L., Yang, B., Ji, G., Zhao, Z., Zhang, H., Wang, F., Huang, P., 2023. Mg/Al layered double hydroxides intercalated with ethylenediamine-tetramethylene phosphonic acid for efficient removal of Pb^{2+} and Cd^{2+} ions and the intercalation mechanism study. Colloids Surf. A: Physicochem. Eng. Asp. 675, 132087. https://doi.org/10.1016/j.colsurfa.2023.132087.

Lin, P., Liu, H., Yin, H., Zhu, M., Luo, H., Dang, Z., 2023. Remediation performance and mechanisms of Cu and Cd contaminated water and soil using Mn/Al-layered double oxide-loaded biochar. J. Environ. Sci. 125, 593–602. https://doi.org/10.1016/J.JES.2022.03.023.

Lu, Y., Yang, P., Li, Y., Wen, D., Wang, S., Wu, F., Fang, L., Pang, Y., 2021. A facile synthesis of nife-layered double hydroxide and mixed metal oxide with excellent microwave absorption properties. Molecules 26 (16), 5046. https://doi.org/10.3390/molecules26165046.

Madhubashani, A.M.P., Giannakoudakis, D.A., Amarasinghe, B., Rajapaksha, A.U., Kumara, P.T.P., Triantafyllidis, K.S., Vithanage, M., 2021. Propensity and appraisal of biochar performance in removal of oil spills: a comprehensive review. Environ. Pollut. 288, 117676. https://doi.org/10.1016/j.envpol.2021.117676.

Manirethan, V., Raval, K., Rajan, R., Thaira, H., Balakrishnan, R.M., 2018. Kinetic and thermodynamic studies on the adsorption of heavy metals from aqueous solution by melanin nanopigment obtained from marine source: pseudomonas stutzeri. J. Env. Manage. 214, 315–324. https://doi.org/10.1016/j.jenvman.2018.02.084.

Mashile, P.P., Mpupa, A., Nomngongo, P.N., 2018. Adsorptive removal of microcystin-LR from surface and wastewater using tyre-based powdered activated carbon: kinetics and isotherms. Toxicon 145, 25–31. https://doi.org/10.1016/j.toxicon.2018.02.044.

Mo, W., He, C., Yang, Y., Cheng, B., Yang, J., Huang, Y., 2024. Adsorption behavior of Mg-Al layered double hydroxide on Pb (II), Zn (II), Cd (II), and As (V) coexisting in aqueous solution. Mater. Today Sustain., 100861 https://doi.org/10.1016/j.mtsust.2024.100861.

Momin, Z.H., Lingamdinne, L.P., Kulkarni, R., Pal, C.A., Choi, Y.L., Chang, Y.Y., Koduru, J.R., 2024. Exploring recyclable alginate-enhanced GCN-LDO sponge for U (VI) and Cd (II) removal: insights from batch and column studies. J. Hazard. Mater. 469, 134015. https://doi.org/10.1016/j.jhazmat.2024.134015.

Mushahary, N., Sarkar, A., Das, B., Rokhum, S.L., Basumatary, S., 2024. A facile and green synthesis of corn cob-based graphene oxide and its modification with corn cob-K2CO3 for efficient removal of methylene blue dye: adsorption mechanism, isotherm, and kinetic studies. J. Indian Chem. Soc. 101 (11), 101409.

Narwal, N., Katyal, D., Kataria, N., Rose, P.K., Warkar, S.G., Pugazhendhi, A., Khoo, K.S., 2023. Emerging micropollutants in aquatic ecosystems and nanotechnology-based

removal alternatives: a review. Chemosphere 341, 139945. https://doi.org/10.1016/j.chemosphere.2023.139945.
Nguyen, T.H., Tran, H.N., Nguyen, T.V., Vigneswaran, S., Trinh, V.T., Nguyen, T.D., Ha Nguyen, T.H., Mai, T.N., Chao, H.P., 2022. Single-step removal of arsenite ions from water through oxidation-coupled adsorption using Mn/Mg/Fe layered double hydroxide as catalyst and adsorbent. Chemosphere 295, 133370. https://doi.org/10.1016/J.CHEMOSPHERE.2021.133370.
Nyaba, L., Matong, J.M., Nomngongo, P.N., 2016. Nanoparticles consisting of magnetite and al2o3 for ligandless ultrasound-assisted dispersive solid phase microextraction of SB, mo and V prior to their determination by ICP-OES. Microchim. Acta 183 (4), 1289–1297. https://doi.org/10.1007/s00604-016-1766-y.
Pastor, A., Rodriguez-Rivas, F., de Miguel, G., Cruz-Yusta, M., Martin, F., Pavlovic, I., Sanchez, L., 2020. Effects of Fe^{3+} substitution on Zn-Al layered double hydroxides for enhanced NO photochemical abatement. Chem. Eng. J. 387, 124110. https://doi.org/10.1016/j.cej.2020.124110.
Qasem, N.A., Mohammed, R.H., Lawal, D.U., 2021. Removal of heavy metal ions from wastewater: a comprehensive and critical review. Npj Clean Water. 4 (1). https://doi.org/10.1038/s41545-021-00127-0.
Saini, A.S., Melo, J.S., 2013. Biosorption of uranium by melanin: kinetic, equilibrium and thermodynamic studies. Bioresour. Technol. 149, 155–162. https://doi.org/10.1016/j.biortech.2013.09.034.
Shafiq, M., Alazba, A.A., Amin, M.T., 2023. Preparation of ZnMgAl-layered double hydroxide and rice husk biochar composites for Cu (II) and Pb (II) ions removal from synthetic wastewater. Water 15 (12), 2207. https://doi.org/10.3390/w15122207.
Shahabi Nejad, M., Sheibani, H., 2022. Super-efficient removal of arsenic and mercury ions from wastewater by nanoporous biochar-supported poly 2-aminothiophenol. J. Environ. Chem. Eng. 10 (3), 107363. https://doi.org/10.1016/j.jece.2022.107363.
Shaikh, W.A., Kumar, A., Chakraborty, S., Naushad, M., Islam, R.U., Bhattacharya, T., Datta, S., 2022. Removal of toxic dye from dye-laden wastewater using a new nanocomposite material: isotherm, kinetics and adsorption mechanism. Chemosphere 308, 136413.
Song, W., Zhang, X., Zhang, L., Yu, Z., Li, X., Li, Y., Yan, L., 2023. Removal of various aqueous heavy metals by polyethylene glycol modified MgAl-LDH: adsorption mechanisms and vital role of precipitation. J. Mol. Liq. 375, 121386. https://doi.org/10.1016/j.molliq.2023.121386.
Šoštarić, T.D., Petrović, M.S., Pastor, F.T., Lončarević, D.R., Petrović, J.T., Milojković, J. V., Stojanović, M.D., 2018. Study of heavy metals biosorption on native and alkali-treated apricot shells and its application in wastewater treatment. J. Mol. Liq. 259, 340–349. https://doi.org/10.1016/j.molliq.2018.03.055.
Sun, Y., Yin, W.M., Wang, Y., Zhao, N.D., Wang, X.Y., Zhang, J.G., Pan, Q.J., 2022. Fabrication of ultra-thin MgAl layered double oxide by cellulose templating and its immobilization effect toward heavy metal ions: cation-exchange and deposition mechanism. Chem. Eng. J. 427, 132017. https://doi.org/10.1016/j.cej.2021.132017.
Thommes, M., Kaneko, K., Neimark, A.V., Olivier, J.P., Rodriguez-Reinoso, F., Rouquerol, J., Sing, K.S., 2015. Physisorption of gases, with special reference to the evaluation of surface area and pore size distribution (IUPAC Technical Report). Pure Appl. Chem. 87 (9–10), 1051–1069. https://doi.org/10.1515/pac-2014-1117.
Tian, Q., Guo, B., Sasaki, K., 2020. Immobilisation mechanism of SE oxyanions in geopolymer: effects of alkaline activators and calcined hydrotalcite additive. J. Hazard. Mater. 387, 121994. https://doi.org/10.1016/j.jhazmat.2019.121994.
Trujillano, R., Rives, V., Rives, R., Rives, B., 2023. Preparation of original and calcined layered double hydroxide as low-cost adsorbents: the role of the trivalent cation on methylene blue adsorption. Molecules 28 (12), 4717. https://doi.org/10.3390/molecules28124717.
Wang, Z., He, G., Chen, Y., Li, X., Ma, J., He, H., 2021. Layered double hydroxide catalysts for ozone decomposition: the synergic role of $M^{2+}$and M^{3+}. Env. Sci. Technol. 56 (2), 1386–1394. https://doi.org/10.1021/acs.est.1c07829.
Wang, D., Repo, E., He, F., Zhang, X., Xiang, H., Yang, W., Zhao, F., 2022. Dual functional sites strategies toward enhanced heavy metal remediation: interlayer expanded Mg-Al layered double hydroxide by intercalation with L-cysteine. J. Hazard. Mater. 439, 129693. https://doi.org/10.1016/j.jhazmat.2022.129693.
Wei, F., Jin, S., Yao, C., Wang, T., Zhu, S., Ma, Y., Song, W., 2023. Revealing the combined effect of active sites and intra-particle diffusion on adsorption mechanism of methylene blue on activated red-pulp pomelo peel biochar. Molecules 28 (11), 4426. https://doi.org/10.3390/molecules28114426.
Xie, Z.H., Zhou, H.Y., He, C.S., Pan, Z.C., Yao, G., Lai, B., 2021. Synthesis, application and catalytic performance of layered double hydroxide based catalysts in advanced oxidation processes for wastewater decontamination: a review. Chem. Eng. J. 414, 128713. https://doi.org/10.1016/j.cej.2021.128713.
Xue, Y., Hou, H., Zhu, S., 2009. Competitive adsorption of copper (II), cadmium (II), lead (II) and zinc (II) onto basic oxygen furnace slag. J. Hazard. Mater. 162 (1), 391–401. https://doi.org/10.1016/j.jhazmat.2008.05.072.
Yang, X., Wan, Y., Zheng, Y., He, F., Yu, Z., Huang, J., Gao, B., 2019. Surface functional groups of carbon-based adsorbents and their roles in the removal of heavy metals from aqueous solutions: a critical review. Chem. Eng. J. 366, 608–621. https://doi.org/10.1016/j.cej.2019.02.119.
Zhang, X., Shan, R., Li, X., Yan, L., Ma, Z., Jia, R., Sun, S., 2021. Effective removal of Cu (II), Pb (II) and Cd (II) by sodium alginate intercalated MgAl-layered double hydroxide: adsorption properties and mechanistic studies. Water Sci. Technol. 83 (4), 975–984. https://doi.org/10.2166/wst.2021.013.
Zhang, Y., Huang, Z., Fang, X., Chen, Y., Fan, S., Xu, H., 2022. Preparation of magnetic porous biochar through hydrothermal pretreatment combined with K_2FeO_4 activation to improve tetracycline removal. Microporous Mesoporous Mater. 343, 112188. https://doi.org/10.1016/j.micromeso.2022.112188. Get rights and content.
Zhang, N., Reguyal, F., Praneeth, S., Sarmah, A.K., 2023a. A novel green synthesized magnetic biochar from white tea residue for the removal of Pb (II) and Cd (II) from aqueous solution: regeneration and sorption mechanism. Environ. Pollut. 330, 121806. https://doi.org/10.1016/j.envpol.2023.121806.
Zhang, X., Liu, T., Zhang, J., Zhu, L., 2023b. Potential mechanism of long-term immobilisation of Pb/cd by layered double hydroxide doped chicken-manure biochar. Int. J. Env. Res Public Health. 20 (1), 867. https://doi.org/10.3390/ijerph20010867.
Zhou, H., Jiang, P., Kuang, Y., Pu, Y., Gan, Y., Yang, Y., 2024. Pb^{2+} and Cd^{2+} ion(s) adsorption capability of a novel hydrotalcite-like absorbent FeMnNi-LTH in water. J. Mol. Liq. 411, 125785. https://doi.org/10.1016/j.molliq.2024.125785.
Zlati, M.L., Georgescu, L.P., Iticescu, C., Ionescu, R.V., Antohi, V.M., 2022. New approach to modelling the impact of heavy metals on the European Union's Water resources. Int. J. Env. Res Public Health. 20 (1), 45. https://doi.org/10.3390/ijerph20010045.